

Theoretical study of the hyperfine interaction constants, Landé *g*-factors, and electric quadrupole moments for the low-lying states of the $^{61}Ni^{q+}$ *(q= 11, 12, 14 ,* and *15)* ions

Ting-Xian Zhang(张婷贤), Yong-Hui Zhang(张永慧), Cheng-Bin Li(李承斌), and Ting-Yun Shi(史庭云)
Citation: Chin. Phys. B, 2021, 30 (**1**): 013101. DOI: 10.1088/1674-1056/abc7a3
Journal homepage: http://cpb.iphy.ac.cn; http://iopscience.iop.org/cpb

What follows is a list of articles you may be interested in

Finite-field calculation of electric quadrupole moments of $^2P_{3/2}$, $^2D_{3/2,5/2}$, and $^2F_{5/2,7/2}$ states for Yb^+ ion

Xi-Tong Guo(郭希同), Yan-Mei Yu(于艳梅), Yong Liu(刘永), Bing-Bing Suo(索兵兵)
Chin. Phys. B, 2020, 29 (**5**): 053101. DOI: 10.1088/1674-1056/ab821c

Ground-state energy of beryllium atom with parameter perturbation method

Feng Wu(吴锋), Lijuan Meng(孟丽娟)
Chin. Phys. B, 2018, 27 (**9**): 093101. DOI: 10.1088/1674-1056/27/9/093101

Forbidden transition properties of fine-structure $2p^3\,^4S_{3/2}$-$2p^3\,^2D_{3/2,5/2}$ for nitrogen-like ions

Xiao-Kang He(何晓康), Jian-Peng Liu(刘建鹏), Xiang Zhang(张祥), Yong Shen(沈咏), Hong-Xin Zou(邹宏新)
Chin. Phys. B, 2018, 27 (**8**): 083102. DOI: 10.1088/1674-1056/27/8/083102

Uncertainty evaluation of the isotope shift factors for $2s2p^{3,1}P_1^o$-$2s^{21}S_0$ transitions in B II

Jianpeng Liu(刘建鹏), Jiguang Li(李冀光), Hongxin Zou(邹宏新)
Chin. Phys. B, 2017, 26 (**2**): 023104. DOI: 10.1088/1674-1056/26/2/023104

Weak- and hyperfine-interaction-induced $1s2s\ ^1S_0 \rightarrow 1s^2\ ^1S_0$ E1 transition rates of He-like ions

Laima Radžiūtė, Erikas Gaidamauskas, Gediminas Gaigalas, Li Ji-Guang, Dong Chen-Zhong, Per Jönsson
Chin. Phys. B, 2015, 24 (**4**): 043103. DOI: 10.1088/1674-1056/24/4/043103

SPECIAL TOPIC — Ultracold atom and its application in precision measurement

Theoretical study of the hyperfine interaction constants, Landé g-factors, and electric quadrupole moments for the low-lying states of the $^{61}Ni^{q+}$ $(q = 11, 12, 14,$ and $15)$ ions*

Ting-Xian Zhang(张婷贤)[1,2], Yong-Hui Zhang(张永慧)[1], Cheng-Bin Li(李承斌)[1,†], and Ting-Yun Shi(史庭云)[1]

[1] State Key Laboratory of Magnetic Resonance and Atomic and Molecular Physics, Wuhan Institute of Physics and Mathematics, Innovation Academy for Precision Measurement Science and Technology, Chinese Academy of Sciences, Wuhan 430071, China

[2] University of Chinese Academy of Sciences, Beijing 100049, China

(Received 9 September 2020; revised manuscript received 20 October 2020; accepted manuscript online 5 November 2020)

Highly charged nickel ions have been suggested as candidates for the ultra-precise optical clock, meanwhile the relevant experiment has been carried out. In the framework of the multiconfiguration Dirac–Hartree–Fock (MCDHF) method, we calculated the hyperfine interaction constants, the Landé g-factors, and the electric quadrupole moments for the low-lying states in the $^{61}Ni^{11+}$, $^{61}Ni^{12+}$, $^{61}Ni^{14+}$, and $^{61}Ni^{15+}$ ions. These states are clock states of the selected clock transitions in highly charged nickel ions (see Fig. 1). Based on discussing the effects of the electron correlations, the Breit interaction, and quantum electrodynamics (QED) effect on these physical quantities, reasonable uncertainties were obtained for our calculated results. In addition, the electric quadrupole frequency shifts and the Zeeman frequency shifts of the clock transitions concerned were analyzed.

Keywords: hyperfine interaction, Landé g-factors, electric quadrupole moment, multiconfiguration Dirac–Hartree–Fock (MCDHF) method

PACS: 31.15.ve, 31.15.vj, 31.15.aj, 32.60.+i **DOI:** 10.1088/1674-1056/abc7a3

1. Introduction

The extraordinary precision of optical clocks allows not only for creating improved time standards, but also for looking for changes in fundamental constants over time, measuring gravity red shift, and probing the existence of forces beyond the Standard Model.[1–3] The fractional uncertainties of a few parts in 10^{-18}, even in 10^{-19}, have been achieved in current leading optical clocks, such as the $^{27}Al^{+}$ clock.[4–7] The dominated uncertainty and frequency shift of the clock transition are caused by the perturbations of the external fields, such as blackbody radiation (BBR) and quadratic Zeeman effect. In comparison to neutral atoms and singly charged ions, the highly charged ions (HCIs) possess optical transitions which can be extremely narrow and less sensitive to the external perturbations, since the electronic cloud is shrunk with the increasing of the ion charge.[8–10] Moreover, the sensitivity of optical transitions in HCIs to effects beyond the Standard Model and Einstein's Theory of Relativity is enhanced by the nuclear charge and ionization degree. Therefore, HCIs are candidates for the novel clock which can improve the accuracy of the optical frequency standards and subsequent researches, such as exploring changes of the fine structure constant α.[11] In recent years, many HCIs have been suggested as the candidates for making ultra-precise optical clocks and exploring new physics beyond the standard model of particle physics.[10] And experimentally, sympathetic cooling and quantum logic spectroscopy of HCIs have been applied for the Ar^{13+} ion,[12,13] which shed light on building the optical clock based on HCIs.

The element nickel (Ni) is abundant in the solar system,[14] and it is also an important impurity element in many tokamak fusion test reactor plasmas. The $3s^23p^5$ $^2P^o_{3/2}$–$^2P^o_{1/2}$ transition of Ni^{11+} ion and the $3s^23p$ $^2P^o_{1/2}$–$^2P^o_{3/2}$ transition in Ni^{15+} ion have appeared in the spectra of the plasma.[15,16] Both transitions above and the other two magnetic dipole (M1) transitions, $3s^23p^4$ $^3P_1$–$^3P_2$ of Ni^{12+} and $3s^23p^2$ $^3P_1$–$^3P_0$ of Ni^{14+}, have been observed in the spectra of the solar corona.[17] In addition, theoretical researches on nickel HCIs mostly focused on transition properties, which are relevant to the emission from the solar, astrophysical, and laboratory plasmas.[18–21] However, in order to analyze the precision spectra and realize HCIs optical clock, calculations on the atomic parameters, such as the hyperfine interaction constants, Landé g-factors, and electric quadrupole moment of the clock states, are necessary.

Several highly charged nickel ions have been proposed

*Project supported by the National Natural Science Foundation of China (Grant Nos. 11704398 and 11934014), the National Key Research and Development Program of China (Grant No. 2017YFA0304402), and the Strategic Priority Research Program of the Chinese Academy of Sciences (Grant No. XDB21030300).

†Corresponding author. E-mail: cbli@wipm.ac.cn

© 2021 Chinese Physical Society and IOP Publishing Ltd

for making ultra-precise optical clock with the fractional uncertainties below 10^{-19} level.[9,22,23] The magnetic dipole (M1) transitions between the states belonging to the configuration of the ground state in the $^{61}Ni^{15+}$ and $^{61}Ni^{14+}$ ions were recommended by Yudin *et al.* The advantages of these ions are the negligible quadrupolar shift, and the simple clock level structures of themself which are benefit to both the theoretical and experimental studies.[9] Soon afterwards, Yu and Sahoo have demonstrated that the projected fractional shift for clock transition $3s^23p\ \ ^2P^o_{3/2}$–$^2P^o_{1/2}$ in the $^{61}Ni^{15+}$ ion is below the 10^{-19} level.[22] They also pointed out that the electric quadrupole (E2) transition $3s^23p^2\ \ ^3P_0$–$^3P_2$ in $^{58}Ni^{12+}$ ion is suitable for making optical clocks, since the quality factor of this transition is larger than 10^{15}, and the M1 transition $3s^23p^2\ ^3P_1$–$^3P_2$ can be used for laser cooling.[23] Recently, the six optical clock transitions (in Fig. 1) in four adjacent charge states of highly charged nickel ions, Ni^{11+}, Ni^{12+}, Ni^{14+}, and Ni^{15+}, have been studied both in theory and experiment. Theoretically, the transition energies, transition rates, and enhancement factors for the α-variation for these clock transitions have been calculated by using the multi-configuration Dirac–Hartree–Fock method (MCDHF). Experimentally, with the achievement of producing and extracting the above ions in the low-energy compact Shanghai–Wuhan Electron Beam Ion Trap,[24] the transition wavelengths of four magnetic-dipole (M1) clock transitions have been measured with an accuracy of tens of ppm, which are in agreement with their calculations.

In this work, using the MCDHF method, we calculate the hyperfine interaction constants, Landé g-factors, and electric quadrupole moment for the states that are involved in the six optical transitions of ^{61}Ni HCIs, as shown in Fig. 1. The active space approach is adopted to investigate the effects of electron correlations on the atomic parameters in detail. The above investigations allow us to obtain high-precision atomic parameters, and to evaluate reliable uncertainties for the present results. We expect our calculations could support the experimental investigations about the highly charged nickel ion optical clock.

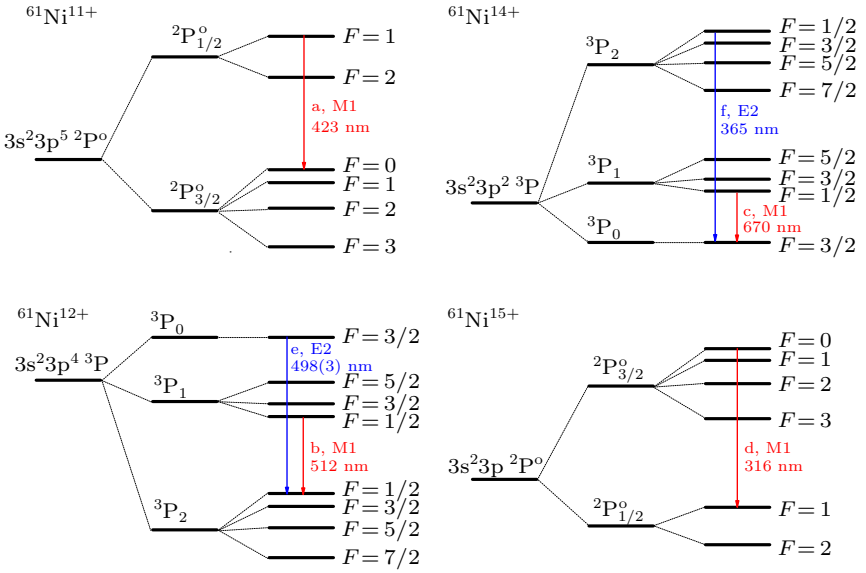


Fig. 1. Partial level structures and clock transitions for $^{61}Ni^{11+}$, $^{61}Ni^{12+}$, $^{61}Ni^{14+}$, and $^{61}Ni^{15+}$ ions. Magnetic-dipole (M1) transitions are shown in red and electric-quadrupole (E2) transitions in blue. The wavelengths labeled in this figure are recommended values by NIST database.[25]

2. Theoretical method

2.1. MCDHF method

Atomic state wave functions (ASFs) in this work are generated by using the MCDHF method.[26,29] For an N-electron atomic system, the Dirac–Coulomb Hamiltonian $H_{\rm DC}$ is given by

$$H_{\rm DC} = \sum_{i=1}^{N}\left[c\,\boldsymbol{\alpha}_i\cdot\boldsymbol{p}_i + (\beta_i - 1)c^2 + V_{\rm nuc}(r_i)\right] + \sum_{i>j}^{N}\frac{1}{r_{ij}}, \quad (1)$$

where c is the speed of light in vaccum, $\boldsymbol{\alpha}_i$ and β_i are the 4×4 Dirac matrices, and $V_{\rm nuc}(r_i)$ is the monopole part of the electron–nucleus interaction. In the MCDHF method, an ASF is constructed by configuration state functions (CSFs) $|\gamma JM_J\rangle$ with the same parity P, total angular momentum J, and its component along the z direction M_J, i.e.,

$$|\Gamma JM_J\rangle = \sum_{i=1}^{N_{\rm CSF}} c_i|\gamma_i JM_J\rangle\,. \quad (2)$$

Here, c_i is the mixing coefficient, and γ_i stands for other appropriate quantum number of the CSF. Every CSF is a linear

combination of products of one-electron Dirac orbitals. The mixing coefficients and the orbitals are optimized simultaneously in the self-consistent field (SCF) procedure to minimize energies of levels concerned. Once a set of orbitals is obtained, the relativistic configuration interaction (RCI) calculations can be carried out to capture more electron correlations by optimizing the mixing coefficients.[27,28] The Breit interaction in the low-frequency approximation

$$B_{ij} = -\frac{1}{2r_{ij}}\left[\boldsymbol{\alpha}_i\cdot\boldsymbol{\alpha}_j + \frac{(\boldsymbol{\alpha}_i\cdot\boldsymbol{r}_{ij})(\boldsymbol{\alpha}_j\cdot\boldsymbol{r}_{ij})}{r_{ij}^2}\right] \tag{3}$$

is included in the RCI Hamiltonian in order to give the correct energy level sequence. In addition, QED corrections are divided into vacuum polarization and self-energy correction and both parts are included in the RCI procedure. The vacuum polarization part is described by the Uehling model potential, and the self-energy correction is given as a sum of the one-electron corrections, which are evaluated by using a screened hydrogenic model.[29,30]

2.2. Hyperfine interaction

The hyperfine interaction is caused by the interaction between the electrons and the electromagnetic multipole moments of the nucleus. The corresponding Hamiltonian is in the form of

$$H_{\rm hfs} = \sum_{k\geq 1}\boldsymbol{T}^{(k)}\cdot\boldsymbol{M}^{(k)}, \tag{4}$$

where the spherical tensor operators, $\boldsymbol{T}^{(k)}$ and $\boldsymbol{M}^{(k)}$ with the rank of k, act on the electronic and nuclear space, respectively.[31] The $k=1$ and $k=2$ terms represent the magnetic dipole and electric quadrupole hyperfine interactions, respectively. The higher-order terms are small and will be neglected in this work. For an N-electrons atom, the electronic tensor operators $\boldsymbol{T}^{(1)}$ and $\boldsymbol{T}^{(2)}$ read

$$\boldsymbol{T}^{(1)} = \sum_{j=1}^{N}\boldsymbol{t}^{(1)}(j) = \sum_{j=1}^{N} -{\rm i}\alpha\left(\boldsymbol{\alpha}_j\cdot\mathbf{l}_j\boldsymbol{C}^{(1)}(j)\right)r_j^{-2}, \tag{5}$$

$$\boldsymbol{T}^{(2)} = \sum_{j=1}^{N}\boldsymbol{t}^{(2)}(j) = \sum_{j=1}^{N} -\boldsymbol{C}^{(2)}(j)r_j^{-3}. \tag{6}$$

Here, i is the imaginary unit, α is the fine-structure constant, $\boldsymbol{C}^{(1)}$ and $\boldsymbol{C}^{(2)}$ are spherical tensor operators, and $\mathbf{l}_j$ is the orbital angular momentum operator. The matrix elements of the nuclear tensor operators $\boldsymbol{M}^{(1)}$ and $\boldsymbol{M}^{(2)}$ are related to the magnetic dipole moment μ_I and electronic quadrupole moment Q of the nucleus with spin I through[32]

$$\mu_I = \langle IM_I = I|\boldsymbol{M}_0^{(1)}|IM_I = I\rangle, \tag{7}$$

$$Q = \langle IM_I = I|\boldsymbol{M}_0^{(2)}|IM_I = I\rangle. \tag{8}$$

The hyperfine interaction couples the electronic angular momentum J and nuclear spin I to a conserved angular momentum F, $\boldsymbol{F} = \boldsymbol{I} + \boldsymbol{J}$. In the first-order approximation, the hyperfine energy correction is given by

$$\Delta E_{\rm hfs} = \frac{1}{2}A_{\rm hfs}C + B_{\rm hfs}\frac{\frac{3}{4}C(C+1) - I(I+1)J(J+1)}{2I(2I-1)J(2J-1)}, \tag{9}$$

where $C = F(F+1) - J(J+1) - I(I+1)$, the magnetic dipole and the electric quadrupole hyperfine interaction constants $A_{\rm hfs}$ and $B_{\rm hfs}$ are[32]

$$A_{\rm hfs}(J) = \frac{\mu_I}{I}\frac{1}{[J(J+1)]^{1/2}}\langle\Gamma J\|\boldsymbol{T}^{(1)}\|\Gamma J\rangle, \tag{10}$$

$$B_{\rm hfs}(J) = 2Q\left[\frac{J(2J-1)}{(J+1)(2J+3)}\right]^{1/2}\langle\Gamma J\|\boldsymbol{T}^{(2)}\|\Gamma J\rangle. \tag{11}$$

2.3. Electric quadrupole moment

Because the atomic charge distribution is not always spherical, there is a deviation from the spherical shape, in which case the atomic state has an electric quadrupole moment. The Hamiltonian for the interaction between the electric quadrupole moment and the electric-field gradient is

$$H_{\rm Q} = \sum_{q=-2}^{2}(-1)^q\nabla\varepsilon_q^{(2)}\Theta_{-q}^{(2)}. \tag{12}$$

The $q=0$ components of the operator $\nabla\varepsilon_q^{(2)}$ and $\Theta_{-q}^{(2)}$ are $\nabla\varepsilon_0^{(2)} = -\frac{1}{2}\frac{\partial\varepsilon_z}{\partial z}$ and $\Theta_0^{(2)} = -\frac{e}{2}\left(3z^2 - r^2\right)$.[33] For a given hyperfine level, the hyperfine energy correction corresponds to $H_{\rm Q}$ is

$$\Delta E_{\rm Q} = \frac{1}{2}\frac{\partial\varepsilon_z}{\partial z}\langle\Gamma JIFM_F|\Theta_0^{(2)}|\Gamma JIFM_F\rangle. \tag{13}$$

The matrix elements in the above formula can be written as

$$\begin{aligned}&\langle\Gamma JIFM_F|\Theta_0^{(2)}|\Gamma JIFM_F\rangle\\ &= (-1)^{I+J+F}\left[3M_F^2 - F(F+1)\right]\sqrt{\frac{2F+1}{(2F+3)(F+1)(2F-1)}}\\ &\quad\times\begin{Bmatrix}J & 2 & J\\ F & I & F\end{Bmatrix}\begin{pmatrix}J & 2 & J\\ -J & 0 & J\end{pmatrix}^{-1}\Theta_J,\end{aligned} \tag{14}$$

where Θ_J is the electric quadrupole moment of the state $|\Gamma J\rangle$

$$\begin{aligned}\Theta_J &= \langle\Gamma JM_J = J|\Theta_0^{(2)}|\Gamma JM_J = J\rangle\\ &= \begin{pmatrix}J & 2 & J\\ -J & 0 & J\end{pmatrix}\langle\Gamma J\|\boldsymbol{\Theta}^{(2)}\|\Gamma J\rangle.\end{aligned} \tag{15}$$

2.4. Zeeman effect of hyperfine level

The Zeeman interaction of the atom with the magnetic field $\boldsymbol{B}$ can be written as[34,35]

$$H_{\rm m} = \left(\boldsymbol{N}^{(1)} + \Delta\boldsymbol{N}^{(1)}\right)\boldsymbol{B} + H_{\rm m}^{\rm nuc}. \tag{16}$$

For an N-electron atom, the electronic tensor operator is

$$\boldsymbol{N}^{(1)} = \sum_{j=1}^{N} \boldsymbol{n}^{(1)}(j) = -\sum_{j=1}^{N} \frac{\sqrt{2}\mathrm{i}}{2\alpha} \Big(\boldsymbol{\alpha}_j \cdot \mathbf{l}_j \boldsymbol{C}^{(1)}(j)\Big) r_j, \quad (17)$$

$$\Delta\boldsymbol{N}^{(1)} = \sum_{j=1}^{N} \Delta\boldsymbol{n}^{(1)}(j) = \sum_{j=1}^{N} \frac{(g_{\mathrm{s}}-2)}{2} \beta_j \boldsymbol{\Sigma}_j, \quad (18)$$

where $\boldsymbol{\Sigma}_j$ is the relativistic spin-matrix, and $g_{\mathrm{s}} = 2.00232$ is the g factor of the electron spin corrected by QED effects. $H_{\mathrm{m}}^{\mathrm{nuc}}$ is the interaction between the nuclear magnetic moment and the magnetic field, which is relate to the nuclear g-factor of $g_I = \mu_I / I\mu_N$ with μ_N being the nuclear magneton.

In the weak-magnetic-field approximation, i.e., $H_{\mathrm{m}} \ll H_{\mathrm{hfs}}$, the energy shift of a given hyperfine level $|FM_F\rangle$ can be calculated, according to the perturbation theory, by

$$\begin{aligned}
\Delta E_{\mathrm{m}}^{(1)} &= \frac{1}{2}\langle \Gamma JIFM_F | \boldsymbol{N}^{(1)} + \Delta\boldsymbol{N}^{(1)} | \Gamma JIFM_F \rangle B \\
&= M_F \frac{F(F+1)+J(J+1)-I(I+1)}{2F(F+1)} \\
&\quad \times \frac{\langle \Gamma J \| \boldsymbol{N}^{(1)} + \Delta\boldsymbol{N}^{(1)} \| \Gamma J \rangle}{\sqrt{J(J+1)}} \\
&= M_F \frac{F(F+1)+J(J+1)-I(I+1)}{2F(F+1)} g_J \frac{B}{2} \\
&= M_F g_F \frac{B}{2}. \qquad (19)
\end{aligned}$$

Here, g_J and g_F are Landé g-factors for the fine and hyperfine states.

3. Computational model

For a many-electron atomic system, the description of electron correlations in the computational model plays a key role on the precision of the calculated atomic parameters. The active space approach is utilized to capture the effect of electron correlations systematically.[30,36] In this approach, the CSFs generated through single (S) and double (D) excitations from the occupied orbitals in the single reference (SR) configuration to virtual orbitals capture the first-order electron correlation effects. In order to achieve high accuracy, the higher-order electron correlations beyond the first-order electron correlation also need to be considered. The CSFs generated through SD excitations from the multireference (MR) configurations set can capture the higher-order electron correlation for the complex atomic system, i.e., MR-SD approach.[37] The MR configurations set is formed by selecting those important CSFs in the first-order ASF. In Table 1, the reference configuration sets, the virtual orbitals, and the number of CSFs corresponding to computational processes of the nickel ions concerned are shown.

For each ion concerned, the computation starts from the Dirac–Hartree–Fock SCF calculation. In this step, the occupied orbitals in the reference configuration are optimized as spectroscopic orbitals (labeled as DHF). As shown in Table 1, the reference configurations for the Ni^{11+}, Ni^{12+}, Ni^{14+}, and Ni^{15+} ions are $3s^23p^5$, $3s^23p^4$, $3s^23p^2$, and $3s^23p$, respectively. The 3s and 3p orbitals are the valence orbitals and others are the core orbitals. In the SCF calculations, the correlation between the valence electrons, VV correlation, and that between the valence electrons and core electrons, CV correlation, are included. The configuration expansions are generated by restricting the SD excitations from the single reference configuration. The restriction to the double excitations is that at most one electron in the core subshell can be substituted at one step. The virtual orbitals are augmented layer by layer up to $n_{\max} = 12$ and $l_{\max} = 6$, $n_{\max}$ and $l_{\max}$ are the maximum principal quantum number and the maximum angular quantum number of the virtual orbitals, and only the last added virtual orbitals are variable in one step. The orbital set obtained in this CV computational model is used for the subsequent RCI calculations. The correlations in the core electrons, referred to as CC correlations, are included in the RCI computation by allowing the SD excitations from the core orbitals to all the virtual orbitals. In order to analyze the effects from different core electrons on the physical quantities under investigation, we open up the core subshell successively. Corresponding models are labeled with CC_{2p}, CC_{2s}, and CC_{1s}, respectively, and the subscripts 2p, 2s, and 1s mean that the CC correlations between these orbitals are involved. So far, the SD-excitation CSFs from the single reference configuration are all included. It means that all the first-order electron correlations are included in our calculations.

As mentioned earlier, the higher-order correlations between the valence orbitals and the core orbitals with $n = 2$ are captured by MR-SD approach. We select the dominant CSFs with the weights of $|c_i| > 0.01$ in the configuration spaces obtained in the CC_{1s} model to form the multireference configuration set and show them in Table 1. To control the number of CSFs, the SD excitations are allowed from orbitals with $n \geq 2$ in the MR configurations to the first three layers of virtual orbitals. These computational models are marked as MR. Finally, the Breit interaction and QED corrections are evaluated based on the MR model. In practice, we employ the GRASP2018[38] package to perform present calculations.

Table 1. The reference configurations sets, the active orbitals (AO) set, and the number of CSFs (NCSF) for the concerned states of the Ni^{11+}, Ni^{12+}, Ni^{14+}, and Ni^{15+} ions in various correlation models. The active orbitals are labelled by the maximum principal quantum number n_{max} and orbital angular momentum l.

Model	AO($n_{max}l$)	NCSF							
		Ni^{11+}		Ni^{12+}		Ni^{14+}		Ni^{15+}	
		Reference configuration							
		$3s^23p^5$		$3s^23p^4$		$3s^23p^2$		$3s^23p$	
		$J=\frac{1}{2}$	$J=\frac{3}{2}$	$J=1$	$J=2$	$J=1$	$J=2$	$J=\frac{1}{2}$	$J=\frac{3}{2}$
DHF	{3s, 3p}	1	1	1	2	1	2	1	1
CV	{12s, 12p, 11d, 12f, 9g, 8h, 7i}	68291	148000	159898	312486	91250	184973	22474	49806
CC_{2p}	{12s, 12p, 11d, 12f, 9g, 8h, 7i}	80205	180496	201566	422682	133458	296074	34775	82854
CC_{2s}	{12s, 12p, 11d, 12f, 9g, 8h, 7i}	90535	206961	235529	508892	167836	382997	45421	109789
CC_{1s}	{12s, 12p, 11d, 12f, 9g, 8h, 7i}	103403	239037	276513	612100	209327	487093	58688	142465
		Multi-reference configurations							
		$3s^23p^5$		$3s^23p^4$		$3s^23p^2$		$3s^23p$	
		$3s3p^53d$		$3s3p^43d$		$3s3p^23d$		$3p^3$	
		$3s^23p^33d^2$		$3s^23p^23d^2$		$3s^23d^2$, $3p^4$		$3s3p3d$	
MR	{6s, 6p, 6d, 6f, 6g, 6h}	827695	2107919	1474046	2784503	708975	1308473	175713	432869

4. Results and discussion

4.1. Hyperfine interaction constants

The calculated magnetic dipole and electric quadrupole hyperfine interaction constants, A_{hfs} and B_{hfs}, for the concerned states of the $^{61}Ni^{11+,12+,14+,15+}$ ions in various correlation models are shown in Table 2. The "MR-B" stands for the results with inclusion of the Breit interaction, and "MR-BQ" with the Breit interaction and QED effect both included. It can be seen that for every hyperfine interaction constant under investigation, the effect of the VV and CV electron correlations is the main contribution. For instance, from the model DHF to CV, the $A_{hfs}(^3P_1)$ of $^{61}Ni^{12+}$ and $^{61}Ni^{14+}$ ions are changed by 37% and 59%, respectively. The effects of the CC correlations on the $A_{hfs}(^3P_1)$ of $^{61}Ni^{12+}$ and $^{61}Ni^{14+}$ ions are 15% and 32%, respectively, and not more than 2% for other hyperfine interaction constants in Table 2. Contributions of the CC correlations mainly result from the correlations among the 2p electrons since there are more electrons in 2p orbitals than those in 2s and 1s orbitals. In addition, we notice that the magnetic dipole hyperfine interaction constants in Table 2 are more sensitive to the CC correlations between 1s orbitals than that between 2s orbitals, although these contributions are quite small. For example, the influences of the CC_{2s} correlations on the $A_{hfs}(^2P^o_{1/2})$ and $A_{hfs}(^2P^o_{3/2})$ of the $^{61}Ni^{11+}$ ion are 0.003% and 0.05%, respectively. While the effects of the CC_{1s} correlations are 0.015% and 0.2%, respectively. The higher-order correlation captured in the MR model cannot be neglected for achieving high precision. The contributions of these correlations are roughly the size of that from the CC correlations, or larger. Additionally, for the $A_{hfs}(^2P^o_{3/2})$ in the $^{61}Ni^{11+,15+}$ ions and the $A_{hfs}(^3P_{1,2})$ in the $^{61}Ni^{12+,14+}$ ions, the effect of the higher-order correlations is opposite to that of the CC correlations. The corrections arisen from the Breit interaction to the $A_{hfs}(^3P_1)$ of $^{61}Ni^{12+,14+}$ ions are about 3%, and it does not exceed 1% to other parameters in Table 2. The contributions of the QED effect are an order of magnitude smaller than that of the Breit interaction.

Computational uncertainty is caused by the electron correlations neglected in the computational model. In this work all the first-order electron correlations and the dominant higher-order correlations are included. The main uncertainty arises from the neglected higher-order correlations related to the 1s electrons. But these effects should be smaller than those from the outer shells because of the stronger nuclear Coulomb potential in the inner region. Conservatively, we treat the contribution of the higher-order correlations captured in the MR model as the uncertainty due to the neglected higher-order correlations. For example, the contribution of the higher-order correlation captured in the MR model to the $A_{hfs}(^2P^o_{1/2})$ of the $^{61}Ni^{11+}$ ions is 0.48%, and it is treated as the uncertainty caused by the neglected higher-order correlations. Additionally, the truncation uncertainty is estimated according to the convergence trends of the various correlations. For example, the truncation uncertainty of $A_{hfs}(^2P^o_{1/2})$ for the $^{61}Ni^{11+}$ ions is 0.03%. The total uncertainty of $A_{hfs}(^2P^o_{1/2})$ for the $^{61}Ni^{11+}$ ions is 0.51%. Yu and Sahoo have calculated the hyperfine interaction constants of the $^{61}Ni^{15+}$ ions by using the relativistic coupled-cluster (RCC) method.[22] Our calculated results are in excellent agreement with theirs. Using the hyperfine interaction constants of the MR-BQ models, we evaluate the transition frequency corrections of the concerned clock transitions in Fig. 1 and show them in Table 3. Accordingly, the changes of the wavelength caused by the hyperfine interaction are about 0.001 nm for the c and d lines, and 0.01 nm for the other lines in Fig. 1.

Table 2. The hyperfine interaction constants $A_{\rm hfs}$ and $B_{\rm hfs}$ (all in MHz) for the concerned states in the $^{61}Ni^{11+}$, $^{61}Ni^{12+}$, $^{61}Ni^{14+}$, and $^{61}Ni^{15+}$ ions. The numbers in the parentheses are the uncertainties for our results.

Model	$A_{\rm hfs}(^2P^o_{1/2})$	$A_{\rm hfs}(^2P^o_{3/2})$	$B_{\rm hfs}(^2P^o_{3/2})$	$A_{\rm hfs}(^3P_1)$	$B_{\rm hfs}(^3P_1)$	$A_{\rm hfs}(^3P_2)$	$B_{\rm hfs}(^3P_2)$
	$^{61}Ni^{11+}$ $3s^23p^5$			$^{61}Ni^{12+}$ $3s^23p^4$			
DHF	−14222	−2658	−1608	237	−838	−2749	1425
CV	−14609	−2790	−1632	149	−849	−2931	1400
CC_{2p}	−14589	−2780	−1630	160	−847	−2916	1399
CC_{2s}	−14590	−2778	−1630	163	−848	−2913	1399
CC_{1s}	−14592	−2773	−1630	171	−848	−2905	1400
MR	−14523	−2791	−1624	129	−845	−2933	1392
MR-B	−14518	−2793	−1621	126	−843	−2940	1400
MR-BQ	−14517(74)	−2792(21)	−1621(9)	126(47)	−843(3)	−2939(34)	1399(9)
	$^{61}Ni^{15+}$ $3s^23p$			$^{61}Ni^{14+}$ $3s^23p^2$			
DHF	−16707	−3128	1893	254	910	−4647	−1175
CV	−17092	−3346	1926	105	927	−5077	−1080
CC_{2p}	−17075	−3325	1924	123	926	−5053	−1077
CC_{2s}	−17079	−3321	1925	128	927	−5049	−1078
CC_{1s}	−17084	−3313	1925	138	927	−5039	−1077
MR	−17027	−3338	1918	96	923	−5073	−1066
MR-B	−17020	−3339	1915	93	921	−5044	−1094
MR-BQ	−17019(54)	−3339(28)	1915(7)	93(44)	921(4)	−5046(36)	−1092(12)
Yu[22]	−17016(66)	−3345(27)	1918(20)				

Table 3. The hyperfine interaction corrections of the transition frequency $\Delta f_{\rm hfs}$ (in MHz) for the clock transitions in Fig. 1. Numbers in parentheses stand for the uncertainties.

Line	Ion	Transition		$\Delta f_{\rm hfs}$
a	Ni^{11+}	$3s^23p^5$	$^2P_{1/2}$ $F=1$–$^2P_{3/2}$ $F=0$	9679(26)
b	Ni^{12+}	$3s^23p^4$	$^3P_1$ $F=1/2$–$^3P_2$ $F=1/2$	15804(20)
c	Ni^{14+}	$3s^23p^2$	$^3P_1$ $F=1/2$–$^3P_0$ $F=3/2$	921(132)
d	Ni^{15+}	$3s^23p$	$^2P_{3/2}$ $F=0$–$^2P_{1/2}$ $F=1$	6356(26)
e	Ni^{12+}	$3s^23p^4$	$^3P_0$ $F=3/2$–$^3P_2$ $F=1/2$	14475(132)
f	Ni^{14+}	$3s^23p^2$	$^3P_2$ $F=1/2$–$^3P_0$ $F=3/2$	15396(132)

4.2. Landé *g*-factor

In Table 4, the *g*-factors of the concerned states in the $^{61}Ni^{11+,12+,14+,15+}$ ions are presented. It can be seen that VV and CV electron correlations make the main contribution to the *g*-factors of all states under investigation. The CC correlations and higher-order correlations make relatively small contributions to the *g*-factors. Take the $^{61}Ni^{11+}$ ion as an example, the effects of VV+CV electron correlations on the $g(^2P^o_{1/2})$ and $g(^2P^o_{3/2})$ are 6.1×10^{-5} and 2.3×10^{-5}, respectively. While the contributions of the CC and higher-order electron correlations are 5.3×10^{-6} and 1.7×10^{-6} for the $^2P^o_{1/2}$ state, 2.7×10^{-6} and 3.2×10^{-6} for the $^2P^o_{3/2}$ state, respectively. It should be stressed that both the CC and higher-order electron correlations should be taken into account in order to evaluate the uncertainties. The influences of the Breit interaction are less than 2 ppm (parts per million) for the *g*-factors in Table 4, except for the $g(^3P_2)$ of the $^{61}Ni^{12+,14+}$ ions, which are 0.1% and 0.2%, respectively. The QED corrections to the *g*-factors are neglected. The uncertainties of the *g*-factors are estimated by using the same method that used in the case of the hyperfine interactions. As show in parentheses in Table 4, the uncertainties are 0.02% and 0.04% for the $g(^3P_2)$ of the $^{61}Ni^{12+}$ and $^{61}Ni^{14+}$ ions, respectively, and less than 0.001% for others. Additionally, the present results are consistent with the calculations of Yu and Sahoo with the RCC method for $g(^2P^o_{1/2,3/2})$ of the $^{61}Ni^{15+}$ ion.

Table 4. The Landé *g*-factors of the concerned states in the $^{61}Ni^{11+}$, $^{61}Ni^{12+}$, $^{61}Ni^{14+}$, and $^{61}Ni^{15+}$ ions. The numbers in the parentheses are the uncertainties for our results.

Model	$g(^2P^o_{1/2})$	$g(^2P^o_{3/2})$	$g(^3P_1)$	$g(^3P_2)$
	Ni^{11+} $3s^23p^5$		Ni^{12+} $3s^23p^4$	
DHF	0.664599	1.333049	1.500123	1.4709
CV	0.664538	1.333026	1.500118	1.4667
CC_{2p}	0.664542	1.333028	1.500119	1.4668
CC_{2s}	0.664543	1.333028	1.500119	1.4668
CC_{1s}	0.664546	1.333029	1.500119	1.4668
MR	0.664545	1.333032	1.500119	1.4665
MR-B	0.664546	1.333032	1.500119	1.4677
MR-BQ	0.664546(6)	1.333032(5)	1.500119(2)	1.4676(3)
	Ni^{15+} $3s^23p$		Ni^{14+} $3s^23p^2$	
DHF	0.664363	1.332872	1.500041	1.4352
CV	0.664301	1.332855	1.500034	1.4244
CC_{2p}	0.664304	1.332856	1.500035	1.4243
CC_{2s}	0.664304	1.332856	1.500035	1.4242
CC_{1s}	0.664305	1.332857	1.500035	1.4242
MR	0.664303	1.332858	1.500037	1.4236
MR-B	0.664302	1.332858	1.500037	1.4265
MR-BQ	0.664302(3)	1.332858(2)	1.500037(2)	1.4262(6)
Yu[22]	0.664536	1.332909		

4.3. Electric quadrupole moments

In Table 5, the electric quadrupole moments of the clock states in the $^{61}Ni^{11+,12+,14+,15+}$ ions are presented. Similar

to the cases of the hyperfine interaction constants and Landé g-factors, the electric quadrupole moments of the states concerned are sensitive to the VV and CV electron correlations as well. The effects of the CC correlations and higher-order correlations on the electric quadrupole moments under investigation are about 1%, and opposite to each other. Thus, to obtain Θ with high precision, both the CC and the higher-order correlation are indispensable. The $\Theta(^3P_2)$ of the Ni^{12+} and Ni^{14+} ions are more sensitive to the Breit interaction and QED effect than other Θ in Table 5. The corrections of the Breit and QED to the $\Theta(^3P_2)$ of the Ni^{12+} ion are 0.95% and 0.06%, respectively, and 3.3% and 0.25% for the Ni^{14+} ion. For other Θ in Table 5, the influences of the Breit and QED effect are less than 0.1% and 0.01%, respectively. Due to the contributions from the neglected higher-order corrections and truncations of the active orbital sets, 1% uncertainties are given for present electric quadrupole moments. Yu and Sahoo[23] have calculated the $\Theta(^3P_2)$ of the Ni^{12+} ion using the DIRAC program that based on Fock space coupled cluster (FSCC) method. Our calculated results agree with their results.

Table 5. The electric quadrupole moments (in a.u.) of the concerned states in the $^{61}Ni^{11+}$, $^{61}Ni^{12+}$, $^{61}Ni^{14+}$, and $^{61}Ni^{15+}$ ions. The numbers in the parentheses are the uncertainties for our results.

	Ni^{11+} $3s^23p^5$	Ni^{12+} $3s^23p^4$		Ni^{14+} $3s^23p^2$		Ni^{15+} $3s^23p$
Model	$\Theta(^2P^o_{3/2})$	$\Theta(^3P_1)$	$\Theta(^3P_2)$	$\Theta(^3P_1)$	$\Theta(^3P_2)$	$\Theta(^2P^o_{3/2})$
DHF	−0.1020	−0.0491	0.0804	0.0457	−0.0552	0.0886
CV	−0.0954	−0.0463	0.0734	0.0436	−0.0468	0.0853
CC_{2p}	−0.0957	−0.0464	0.0737	0.0438	−0.0470	0.0856
CC_{2s}	−0.0958	−0.0465	0.0737	0.0439	−0.0471	0.0858
CC_{1s}	−0.0959	−0.0465	0.0738	0.0440	−0.0471	0.0859
MR	−0.0952	−0.0462	0.0732	0.0438	−0.0466	0.0858
MR-B	−0.0952	−0.0463	0.0739	0.0438	−0.0482	0.0858
MR-BQ	−0.0952(2)	−0.0463(3)	0.0738(7)	0.0438(2)	−0.0481(5)	0.0858(1)
Yu			0.07325*[23]			0.0853(11)[22]

*The values given in the last line are obtained by the results shown in Table II of Ref. [23] divided by two, according to the definition of the Θ_J used in this work.

4.4. Electric quadrupole shift

The electric quadrupole shift caused by the interaction between the electric quadrupole moments of the clock states with the gradient of the electric field is one of the main systematic shifts in the atomic clock. For the isotopes with nonzero nuclear spin, the quadrupole shift can be either eliminated or strongly suppressed by choosing clock transitions between the hyperfine levels which make the 6j symbol in Eq. (14) equal to zero. For the $^{61}Ni^{11+}$ and $^{61}Ni^{15+}$ ions, it is proper to choose the transitions between $^2P^o_{3/2}$ $F=0$ and $^2P^o_{1/2}$ $F=1,2$. In the $^{61}Ni^{12+}$ and $^{61}Ni^{14+}$ ions, the suitable states are $^3P_0$ $F=3/2$, $^3P_1$ $F=1/2$, and $^3P_2$ $F=1/2$. Since $\Theta^{(2)}_{-q}$ is an even-parity operator of rank 2, the electric quadrupole moments of the states with $F<1$ are zero according to the selection rules. Thus, for the M1 clock transition in $^{61}Ni^{12+}$, $^3P_1$ $F=1/2$–$^3P_2$ $F=1/2$, the quadrupolar shift is zero identically. For the other clock transitions concerned, the electric quadrupolar shifts are suppressed, which are benefited from that the Θ_J of the $^2P^o_{1/2}$ and $^3P_0$ states are zero. Moreover, the electric quadrupole shift can be canceled by two methods experimentally. Both of them are based on measuring the Zeeman spectrum of the clock transition.[33,39] The averaged value of the transition frequencies that correspond to three magnetic fields with the same magnitude but with mutually perpendicular directions does not contain the electric quadrupole shift. Alternatively, the electric quadrupole shift can be eliminated when an average over all M_F is done.

4.5. Zeeman shift

The Zeeman shift of the clock transition frequency is caused by the residual magnetic field $\boldsymbol{B}$ of the environment. Generally, it is sufficient to consider only the first and second-order Zeeman effects on the clock transitions frequency. The first-order Zeeman shift can be canceled by measuring two transitions with opposite magnetic quantum number M_F and averaging the frequencies.[40] Indeed, for the clock transitions between the sublevels $^2P^o_{1/2}$ $F=0$ $M_F=0$ and $^2P^o_{3/2}$ $F=1,2$ $M_F=0$ of the $^{61}Ni^{11+,15+}$ ions, the first-order Zeeman shift equals zero. The quadratic Zeeman shift can be evaluated by $\Delta E^{(2)}_m = C_{M2}B^2$, where $C_{M2} \sim (g_J\mu_B - g_I\mu_N)/h^2A_{hfs}$. Using the calculated Landé g-factors and magnetic dipole hyperfine interaction constants, we estimate the C_{M2} for the clock transitions investigated in this work, and the values are listed in the third column of Table 6. Table 6 also gives the transition frequencies of the clock transitions concerned which are $\sim 10^{14}$ Hz. By assuming a small magnetic field $B=1$ μT, the relative quadratic Zeeman shifts are evaluated. From Table 6, it can be seen that the quadratic Zeeman shifts are non-negligible for the six clock transitions concerned, and we must identify the shifts precisely. The g-factor plays a key role in

the accurate diagnosis of the magnetic field strength, which is necessary for determining the quadratic shift precisely.

Table 6. The quadratic Zeeman shift coefficients C_{M2} (in Hz/T^2) and the transition frequencies f (in Hz) of the concerned clock transitions in the ^{61}Ni^{11+}, ^{61}Ni^{12+}, ^{61}Ni^{14+}, and ^{61}Ni^{15+} ions. The relative quadratic Zeeman shifts are evaluated by assuming a small magnetic field $B = 1$ μT. Numbers in square brackets stand for the power of 10.

Ion	Transition	C_{M2} (Hz/T^2)	f (Hz)	$\Delta E_m^{(2)}/f$
Ni^{11+}	^{2}P$^o_{1/2}$–^{2}P$^o_{3/2}$	1.2[11]	7.1[14]	1.7[−16]
Ni^{12+}	^{3}P$_1$–^{3}P$_2$	3.6[12]	5.9[14]	6.2[−15]
Ni^{12+}	^{3}P$_1$–^{3}P$_2$	1.4[11]	6.0[14]	2.4[−16]
Ni^{14+}	^{3}P$_1$–^{3}P$_0$	4.7[12]	4.5[14]	1.1[−14]
Ni^{14+}	^{3}P$_2$–^{3}P$_0$	7.9[10]	8.2[14]	9.6[−17]
Ni^{15+}	^{2}P$^o_{3/2}$–^{2}P$^o_{1/2}$	9.9[10]	8.3[14]	1.2[−16]

5. Conclusion

In summary, we calculated the hyperfine interaction constants, Landé g-factors, and electric quadrupole moments of the sates involved in the clock transitions in ^{61}Ni^{11+}, ^{61}Ni^{12+}, ^{61}Ni^{14+}, and ^{61}Ni^{15+} ions using the MCDHF method. Based on the active space approach, the effects of the electron correlations, the Breit interaction, and QED effect on the above atomic parameters were discussed. We found that the VV and CV electron correlations make significant contributions to these physical quantities concerned. Moreover, both the CC and higher-order electron correlations should be included in order to acquire high precision atomic parameters. Reliable uncertainties were evaluated by taking into account the contributions from the neglected high-order corrections and truncations effects of the active orbital sets. In addition, we discussed the electric quadrupole shifts and Zeeman shifts of the clock transitions concerned. For the clock transitions under investigation, the electric quadrupole shifts and linear Zeeman shifts can be eliminated or suppressed. While the quadratic Zeeman shifts should be measured precisely for achieving the uncertainty below the 10^{-19} level.

Acknowledgment

We would like to thank Li Ji-Guang of Institute of Applied Physics and Computational Mathematics for many useful discussions.

References

[1] Ludlow A D, Boyd M M, Ye J, Peik E and Schmidt P O 2015 *Rev. Mod. Phys.* **87** 637
[2] Rosenband T, Hume D B, Schmidt P O, Chou C W, Brusch A, Lorini L, Oskay W H, Drullinger R E, Fortier T M, Stalnaker J E, Diddams S A, Swann W C, Newbury N R, Itano W M, Wineland D J and Bergquist J C 2008 *Science* **319** 1808
[3] Godun R M, Nisbet-Jones P B R, Jones J M, King S A, Johnson L A M, Margolis H S, Szymaniec K, Lea S N, Bongs K and Gill P 2014 *Phys. Rev. Lett.* **113** 210801
[4] Chou C W, Hume D B, Koelemeij J C J, Wineland D J and Rosenband T 2010 *Phys. Rev. Lett.* **104** 070802
[5] Nicholson T L, Campbell S L, Hutson R B, Marti G E, Bloom B J, McNally R L , Zhang W, Barrett M D, Safronova M S, Strouse G F, Tew W L and Ye J 2015 *Nat. Commun.* **6** 6896
[6] Huntemann N, Sanner C, Lipphardt B, Tamm Chr and Peik E 2016 *Phys. Rev. Lett.* **116** 063001
[7] Brewer S M, Chen J S, Hankin A M, Clements E R, Chou C W, Wineland D J, Hume D B and Leibrandt D R 2019 *Phys. Rev. Lett.* **123** 033201
[8] Derevianko A, Dzuba V A and Flambaum V V 2012 *Phys. Rev. Lett.* **109** 180801
[9] Yudin V I, Taichenachev A V and Derevianko A 2014 *Phys. Rev. Lett.* **113** 233003
[10] Kozlov M G, Safronova M S, Crespo López-Urrutia J R and Schmidt P O 2018 *Rev. Mod. Phys.* **90** 045005
[11] Berengut J C, Dzuba V A and Flambaum V V 2010 *Phys. Rev. Lett.* **105** 120801
[12] Micke P, Leopold T, King S A, Benkler E, Spieß L J, Schmöger L, Schwarz M, Crespo López-Urrutia J R and Schmidt P O 2020 *Nature* **578** 60
[13] Schmöger L, Versolato O O, Schwarz M, Kohnen M, Windberger A, Piest B, Feuchtenbeiner S, Pedregosa-Gutierrez J, Leopold T, Micke P, Hansen A K, Baumann T M, Drewsen M, Ullrich J, Schmidt P O and Crespo López-Urrutia J R 2015 *Science* **347** 1233
[14] Asplund M, Grevesse N, Sauval A J and Scott P 2009 *Annu. Rev. Astron. Astrophys.* **47** 481-522
[15] Hinnov E, Denne B, Ramsey A, Stratton B and Timberlake J 1990 *J. Opt. Soc. Am. B* **7** 2002
[16] Behringer K H, Carolan P G, Denne B, Decker G, Engelhardt W, Forrest M J, Gill R, Gottardi N, Hawkes N C, Källne E, Krause H, Magyar G, Mansfield M, Mast F, Morgan P, Peacock N J, Stamp M F and Summers H P 1986 *Nucl. Fusion* **26** 751
[17] Jefferies J T, Orrall F Q and Zirker J B 1971 *Sol. Phys.* **16** 103
[18] Ekaman J, Jönsson P, Radžiūtė L,Gaigalas G, Del Zanna G and Grant I P 2018 *At. Data Nucl. Data Tables* **120** 152
[19] Del Zanna G and Badnell N R 2016 *Astron. Astrophys.* **585** A118
[20] Nazir R T, Bari M A, Bilal M, Sardar S, Nasim M H and Salahuddin M 2017 *Chin. Phys. B* **26** 023102
[21] Bilal M, Berrwerth R, Volotka A V and Fritzsche S 2017 *Mon. Not. R. Astron. Soc.* **469** 4620
[22] Yu Y M and Sahoo B K 2016 *Phys. Rev. A* **94** 062502
[23] Yu Y M and Sahoo B K 2018 *Phys. Rev. A* **97** 041403(R)
[24] Liang S Y, Lu Q F, Wang X C, Yang Y, Yao K, Shen Y, Wei B R, Xiao J, Chen S L, Zhou P P, Sun W, Zhang Y H, Huang Y, Guan H, Tong X, Li C B, Zou Y M, Shi T Y and Gao K L 2019 *Rev. Sci. Instrum.* **90** 093301
[25] Kramida, A, Ralchenko, Yu, Reader, J and NIST ASD Team 2019 *NIST Atomic Spectra Database* (version 5.7.1)
[26] Grant I P 2007 *Relativistic quantum theory of atom and molecules* (New York: Springer)
[27] Liu J P, Li J G and Zou H X 2017 *Chin. Phys. B* **26** 023104
[28] He X K, Liu J P, Zhang X, Shen Y and Zou H X 2018 *Chin. Phys. B* **27** 083102
[29] Fischer C F, Godefroid M, Brage T, Jönsson P and Gaigalas G 2016 *J. Phys. B: At. Mol. Opt. Phys.* **49** 182004
[30] Li J G, Jönsson P, Godefroid M, Dong C and Gaigalas G 2012 *Phys. Rev. A* **86** 052523
[31] Lindgren I 1984 *Rep. Prog. Phys.* **47** 345
[32] Jönsson P, Parpia F A and Fischer C F 1996 *Comput. Phys. Commun.* **96** 301
[33] Itano W M 2000 *J. Res. Natl. Inst. Stand. Technol.* **105** 829
[34] Cheng K T and Childs W J 1985 *Phys. Rev. A* **31** 2775
[35] Andersson M and Jönsson P 2008 *Comput. Phys. Commun.* **178** 156
[36] Bieroń J, Fischer C F , Indelicato P, Jönsson P and Pyykkö P 2009 *Phys. Rev. A* **79** 052502
[37] Li J G, Godefroid M and Wang J G 2016 *J. Phys. B: At. Mol. Opt. Phys.* **49** 115002
[38] Fischer C F, Gaigalas G, Jönsson P and Bieroń J. 2019 *Comput. Phys. Commun.* **237** 184
[39] Dubé P, Madej A A, Bernard J E, Marmet L, Boulanger J S and Cundy S 2005 *Phys. Rev. Lett.* **95** 033001
[40] Itano W M, Bergquist J C, Rosenband T, Wineland D J, Hume D, Chou C W, Jefferts S R, Heavner T P, Parker T E, Diddams S A and Fortier T M 2010 *Laser Spectroscopy* (Singapore: World Scientific) p. 117